Mon. Not. R. astr. Soc. (1969) **145**, 271–295.

NUMERICAL CALCULATIONS OF THE DYNAMICS OF A COLLAPSING PROTO-STAR*

Richard B. Larson

(Communicated by P. Demarque)

(Received 1969 February 4)

SUMMARY

Numerical calculations of the dynamics of a spherically symmetric collapsing proto-star of one solar mass have been made for various initial conditions. Calculations have also been made for masses of $2M_\odot$ and $5M_\odot$. In all cases the collapse is found to be extremely non-homologous and is such that a very small part of the cloud's mass at the centre reaches stellar densities and stops collapsing before most of the cloud has had time to collapse very far. The stellar core thus formed subsequently grows in mass as material falls into it, finally becoming an ordinary star when all of the proto-stellar material has been accreted. During most of this time the stellar core is completely obscured by the dust in the infalling cloud, the absorbed radiation reappearing in the infra-red as thermal emission from the dust grains. The resulting star is almost a conventional Hayashi pre-main sequence model, but it appears rather low on the Hayashi track. For masses much greater than about $2M_\odot$ the convective Hayashi phase does not exist at all. It appears that certain properties of T Tauri stars may find explanation in the results of the present calculations.

In an appendix to the paper it is shown that limiting forms may be derived for the density and velocity distributions near the centre of an isothermally collapsing sphere. This may be shown to be possible also for a sphere with a polytropic equation of state. Numerical results are presented for the limiting solution in the isothermal case.

1. INTRODUCTION

The problem of the dynamical collapse of a proto-star under its own self-gravitation has recently been considered by a number of authors, including Gaustad (1963), Hayashi & Nakano (1965) and Hayashi (1966). These authors did not actually solve the equations governing the collapse, which can only be done numerically, but attempted to deduce the main features of the collapse by introducing a number of simplifying assumptions; for example, it has often been assumed that the collapse is roughly homologous and that the density distribution in the collapsing proto-star can be adequately approximated by a polytropic density distribution. It has been the purpose of the present investigation to dispense with some of these assumptions and solve numerically the hydrodynamical equations governing the collapse, with the aim of computing in detail the evolution of a proto-star as it collapses under its self-gravitation.

* Based on a Ph.D. Thesis submitted at the California Institute of Technology (1968), which may be consulted for more details. Copies of the thesis are available from University Microfilms, Ann Arbor, Michigan 48106 (order no. 68-13,070).

Since very little is known about the circumstances under which star formation begins, it is necessary to start with a number of more or less arbitrary assumptions. Our approach will be to consider a spherical volume of interstellar material having a specified mass, usually one solar mass, and to follow its collapse from simple assumed initial conditions. In order for this material to collapse gravitationally, its initial density must be above a certain minimum value which for one solar mass is several orders of magnitude higher than typical interstellar densities. We do not consider the problem of the formation of a cloud with this high density, but simply assume that such a cloud must form at some stage in the course of star formation. In view of the many uncertainties, we have for the most part not considered it worthwhile in this project to use other than the simplest possible assumptions for the initial and boundary conditions for the collapsing cloud.

In Sections 2 and 3 we describe the various assumptions and approximations which we have adopted in the present calculations, and in Section 4 we describe the results of a collapse calculation for a proto-star of one solar mass made using these assumptions. In Section 5 we describe the results of some further collapse calculations in which certain of the assumptions and input parameters have been changed in order to test their importance for the results. In Section 6 we summarize the important results of the present calculations and indicate the possible relation between our results and certain properties of T Tauri stars.

2. ASSUMPTIONS AND INPUT DATA

(a) *General assumptions*

In previous work it has generally been assumed for simplicity that the collapse of a proto-star is spherically symmetrical, and rotation, magnetic fields, and internal turbulent motions have been neglected. In order to keep the numerical calculations tractable, we have retained these assumptions in the present work. In reality some of the neglected effects, particularly rotation, are almost certainly important, so the resulting model is clearly highly idealized and may not be at all realistic.

(b) *Composition of the proto-stellar material*

We assume, following Gaustad (1963), that we are dealing with star formation in an H I region with typical Population I composition, and we adopt Gaustad's composition parameters. We assume that, at the rather high densities ($\gtrsim 10^{-19}$ g cm^{-3}) required for the collapse of a proto-star of one solar mass, the hydrogen is essentially all in molecular form. Dust grains are assumed to exist with the properties adopted by Gaustad; the dust then constitutes roughly 1 per cent of the total mass of the material.

(*c*) *Opacity*

The opacity of the proto-stellar material has been discussed by Gaustad (1963), and Rosseland mean opacities based on Gaustad's data have been tabulated by Hayashi & Nakano (1965). Gaustad found that as long as dust grains exist at all, they are by far the dominant source of opacity. Despite the work of Gaustad, however, the nature and infra-red absorption properties of the dust grains must still be considered as quite uncertain, particularly at the higher temperatures where the more volatile grain constituents such as H_2O evaporate. Consequently

we have not considered it worthwhile in this project to represent in detail the variation of opacity with temperature indicated by Gaustad's data, but have instead used a simple constant value for the Rosseland mean opacity: $\kappa_R = 0{\cdot}15 \text{cm}^2\,\text{g}^{-1}$. The dust grains have been assumed to evaporate at a temperature of 1400°K.

When the dust grains evaporate, the Rosseland mean opacity drops by a large factor and molecular absorption then becomes an important contributor to the opacity at temperatures up to about 3000°K (Tsuji 1966). For the present purposes, however, the opacity in this temperature range is not very important and the opacities of Cox (1966) for $T \geq 1500$°K appear to be adequate. In order to avoid certain numerical difficulties associated with a discontinuous drop in opacity at the dust evaporation temperature, we have used a logarithmically linear interpolation of the opacity between 1400°K and 2000°K; the Cox opacities have then been used for $T \geq 2000$°K.

(d) *Temperature*

At the high densities relevant for the collapse of a proto-star of one solar mass, the dominant heating effect is expected to be compressional heating of the material as it collapses gravitationally at approximately the free-fall rate, and the dominant cooling processes are expected to be collisional transfer of energy from gas molecules to dust grains and radiative cooling of the dust grains. We have calculated the temperature resulting from these heating and cooling effects and we find, in approximate agreement with Hayashi (1966), that the temperature remains nearly constant at about 10°K over the whole density range from the minimum density required to ensure gravitational collapse ($\sim 10^{-19}$ g cm^{-3}) to the density at which the central part of the cloud becomes optically thick ($\sim 10^{-13}$ g cm^{-3}). Accordingly we have assumed that initially and throughout the early optically thin stages of the collapse the proto-stellar cloud is isothermal at a temperature of 10°K.

(e) *Boundary conditions*

For the boundary condition on the collapsing proto-star we have in most cases adopted the simplest assumption, namely that the outer boundary of the cloud remains fixed in space at a constant radius. This corresponds to allotting a constant volume to each collapsing proto-star in a proto-cluster or region of star formation. In the lack of further knowledge about star formation, it would appear difficult to justify any other assumption as more realistic.

(f) *Initial conditions*

For the initial conditions we have again adopted the simplest assumptions, namely that the cloud starts from rest with a uniform density distribution. With our choice of initial and boundary conditions, the maximum cloud radius for which gravitational collapse will occur has been found from trial collapse calculations to be given by

$$R_{\max} = 0{\cdot}46 \frac{GM}{\mathscr{R}T} \qquad (1)$$

where G is the gravitational constant, M is the mass of the cloud, and $\mathscr{R}$ is the gas constant. For $R > R_{\max}$ the cloud starts to collapse, but soon rebounds and then oscillates about an equilibrium configuration without ever collapsing to a

star. It was found in practice that if the calculations were started with a value of R very close to $R_{\max}$, small inaccuracies in the calculations could cause the cloud to rebound instead of collapse to a star. In order to avoid this difficulty, we have set the cloud radius equal to the slightly smaller value

$$R_c = 0{\cdot}41 \frac{GM}{\mathscr{R}T} \tag{2}$$

which according to the work of McCrea (1957) and others is small enough to ensure collapse from arbitrary starting conditions. With $M = M_\odot$, $T = 10\,^\circ\mathrm{K}$, and $\mathscr{R} = 3{\cdot}36 \times 10^7$ erg $\mathrm{g}^{-1}\,^\circ\mathrm{K}^{-1}$ as appropriate for Gaustad's composition, we obtain $R_c = 1{\cdot}63 \times 10^{17}$ cm, corresponding to an initial cloud density of $1{\cdot}10 \times 10^{-19}$ g cm^{-3}.

The importance of the assumed initial and boundary conditions has been tested in a number of calculations by the author in which various kinds of initial and boundary conditions have been tried; similar calculations have also been made by Penston (1966) and Bodenheimer & Sweigart (1968). It appears from these calculations that the main features of the collapse are qualitatively much the same in all cases, regardless of the details of the initial and boundary conditions. Consequently the choice of initial and boundary conditions does not appear to be of critical importance, at least as far as the qualitative features of the results are concerned.

3. EQUATIONS AND APPROXIMATIONS

The present calculations have been done mostly with Eulerian or modified Eulerian computational schemes; accordingly we give below the equations of gasdynamics and radiation transfer in Eulerian form. These equations are valid as long as the material is optically thick and as long as convective energy transport does not become important.

$$\frac{\partial m}{\partial t} + \frac{4\pi r^2 u}{V} = 0 \tag{3}$$

$$\frac{\partial u}{\partial t} + u\frac{\partial u}{\partial r} + \frac{Gm}{r^2} + V\frac{\partial P}{\partial r} = 0 \tag{4}$$

$$\frac{\partial E}{\partial t} + P\frac{\partial V}{\partial t} + u\left(\frac{\partial E}{\partial r} + P\frac{\partial V}{\partial r}\right) + \frac{3}{4\pi}V\frac{\partial L}{\partial r^3} = 0 \tag{5}$$

$$\frac{1}{V} - \frac{3}{4\pi}\frac{\partial m}{\partial r^3} = 0 \tag{6}$$

$$L = -\frac{64\pi\sigma}{3} r^2 \frac{VT^3}{\kappa}\frac{\partial T}{\partial r}. \tag{7}$$

In these equations m is the mass within a sphere of radius r, u is the flow velocity, $V \equiv 1/\rho$ is the specific volume, E is the specific internal energy, σ is the Stefan–Boltzmann constant, and κ is the Rosseland mean opacity; the other symbols have their usual meanings. For the two non-trivial boundary conditions which must be specified at the outer boundary $r = R$, we have taken $u = 0$ (corresponding to a fixed boundary) and $T = 10\,^\circ\mathrm{K}$.

The use of the radiation diffusion equation (7) requires some discussion, since we have used this equation even when the material is optically thin and the diffusion

equation is physically inapplicable. During the initial optically thin stages of the collapse, the use of the diffusion equation has the effect of artificially holding the temperature isothermal at the assumed boundary temperature of 10°K. In reality the temperature during this phase of the collapse is expected to remain nearly constant at 10°K anyway; thus the use of the diffusion equation may in fact provide a reasonably good approximation to reality. During the later stages of the collapse the situation is less favourable, since the luminosity from the central part of the cloud begins to heat up the outer optically thin parts of the cloud; the temperatures calculated with the diffusion equation then become much too low in this region. Over most of the cloud, this error is of little consequence for the dynamics, since the material is very nearly in free fall anyway. Near the outer boundary of the cloud the error may become significant, since if the temperature were correctly calculated the pressure force might become sufficient to retard or prevent the collapse of the outermost part of the cloud. It does not appear, however, that this would seriously alter our main conclusions.

During the early stages of the collapse, shock fronts have been treated by the standard artificial viscosity method, which allows shock fronts to be handled automatically wherever they may arise in the flow, without the need for a special treatment. During the later stages of the collapse, however, it becomes necessary to abandon the artificial viscosity method and use a 'shock fitting' technique in which the shock front is treated as a discontinuous jump in the flow variables. It also becomes essential to take into account radiative energy transfer in the shock front; the ordinary adiabatic shock jump conditions cannot be used. We have not attempted to solve in detail the difficult problem of the radiative transfer in the shock front, but have instead used some very simple approximations which appear to be adequate for the present purposes; these are derived and discussed in Appendix A.

During the later stages of evolution of a proto-star, convective energy transport becomes important. To take this into account we have used a simplified form of the conventional mixing length treatment of convection. The mixing length has been set equal to the density scale height, and the velocity of convection has not been calculated but has been treated as an arbitrary parameter, for which a value of 1 km s^{-1} has usually been used.

In view of the many uncertainties involved in this project, we have not considered it worthwhile to seek results of high numerical accuracy, and the calculations have accordingly been made with rather coarse space and time grids. A general level of accuracy of the order of 20 per cent or so was considered a reasonable goal; various checks have verified that numerical accuracies of this order were indeed generally attained.

4. RESULTS

(a) *Initial isothermal phase*

Initially there are no pressure gradients in the cloud, so the whole cloud begins to collapse in free fall. As the material falls inward, the density near the boundary of the cloud drops, while the density in the interior of the cloud rises; consequently a pressure gradient arises in the outer part of the cloud, causing the collapse in this region to be significantly retarded from a free fall. The density therefore rises more rapidly at the centre than in the outer parts of the cloud,

and the density distribution becomes peaked at the centre. The collapse of the central part of the cloud continues approximately as a free fall (even though pressure gradients are *not* negligible), and since the free-fall time depends inversely on the density, the collapse proceeds most rapidly at the centre where the density is highest; thus the density distribution becomes more and more sharply peaked at the centre as the collapse proceeds.

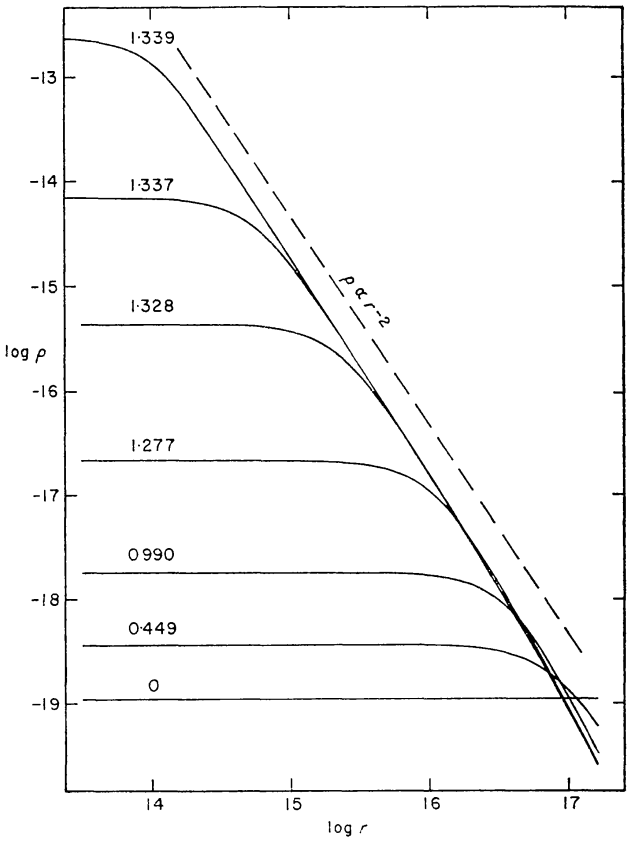

FIG. 1. *The variation with time of the density distribution in the collapsing cloud (CGS units). The curves are labelled with the times in units of* 10^{13} *s since the beginning of the collapse. Note that the density distribution closely approaches the form* $\rho \propto r^{-2}$.

The development of the central density peak during the initial isothermal phase of the collapse is illustrated in Fig. 1. It is evident in this diagram that as the collapse proceeds the major changes in density occur in a smaller and smaller region near the centre and on a shorter and shorter time scale, while practically nothing happens in the outer parts of the cloud. At the latest time shown, the width of the central density peak is only about 10^{-3} times the cloud radius, and the mass contained in this region is also only about 10^{-3} times the total mass. This extremely non-homologous character of the collapse is found to occur regardless of the choice of initial and boundary conditions, and has been found also in the calculations of Penston (1966) and Bodenheimer & Sweigart (1968).

(b) *Formation of the opaque core*

When the central density reaches about 10^{-13} g cm^{-3}, a small region at the centre of the cloud starts to become opaque; the heat generated by the collapse

in this region is then no longer freely radiated away, and the compression becomes approximately adiabatic. The central temperature and pressure then begin to rise rapidly, soon becoming sufficient to decelerate and stop the collapse at the centre. There then arises a small central ' core ' in which the material has stopped collapsing and is approaching hydrostatic equilibrium. Outside this core, the material is still nearly isothermal and continues to fall inward almost in free fall; consequently a shock front arises at the boundary of the core, where the infalling material is suddenly stopped. The initial mass and radius of the core are about 10^{31} g and 6×10^{13} cm, respectively, and the central density and temperature at this time are about 2×10^{-10} g cm^{-3} and 170°K, respectively.

When the material at the centre of the core first stops collapsing there is a rebound, followed by a series of radial oscillations of the core about an equilibrium configuration. The rebound and the ensuing pulsations are however not very large in amplitude (about 10–20 per cent in radius), and do not appear to be of any importance for the subsequent evolution of the core. As the collapse proceeds, the core grows in mass due to the infall of the surrounding material; at the same time, however, the core radius decreases because of radiative energy losses from the outer layers of the core. Thus the shock front bounding the core actually moves inward in radius, although it moves outward in mass.

(c) *Formation of the second (stellar) core*

After the core mass has increased by about a factor of 2 and the radius has decreased by a similar factor, the central temperature reaches a value of about 2000°K, at which point the hydrogen molecules begin to dissociate. This reduces the ratio of specific heats γ below the critical value 4/3, with the result that the material at the centre of the core becomes unstable and begins to collapse dynamically. Most of the energy generated by this collapse goes into the dissociation of H_2 molecules, so that the temperature rises only slowly with increasing density; the situation is thus similar to the earlier isothermal collapse of the whole cloud. In this second dynamical collapse phase, as in the first, the density distribution in the collapsing region becomes more and more sharply peaked at the centre, and the time scale becomes shorter and shorter with increasing central density.

The central collapse of the core continues until the hydrogen molecules are nearly all dissociated and γ again rises above 4/3. The central pressure then rises rapidly and once again becomes sufficient to decelerate and stop the collapse at the centre. A small central core in hydrostatic equilibrium then arises, bounded by a shock front in which the surrounding infalling material is suddenly stopped. When this second core forms there is again a small rebound, followed by a series of radial pulsations of the core. The initial mass and radius of the second core are about 3×10^{30} g ($1\cdot5\times10^{-3}\,M_\odot$) and 9×10^{10} cm ($1\cdot3\ R_\odot$) respectively, and the central density and temperature are about 2×10^{-2} g cm^{-3} and 2×10^{4}°K, respectively.

At the time of formation of the second core, the outer part of the first core has not yet had time to collapse very far since the central collapse began, and the first shock front is still in existence. The density and velocity distributions throughout the cloud at a time shortly after the formation of the second core are illustrated in Fig. 2. Because of the smoothing effects of the artificial viscosity method used in the calculations, the shock fronts appear in this diagram not as discontinuities

in the flow variables, but most conspicuously as regions of steep positive slope in the velocity curve.

(d) *Expansion of the stellar core*

When the second core first forms, the density in its vicinity is so high that the material is quite opaque, and radiative energy transport is negligible. Thus the shock front forming its boundary is initially adiabatic. As material falls into

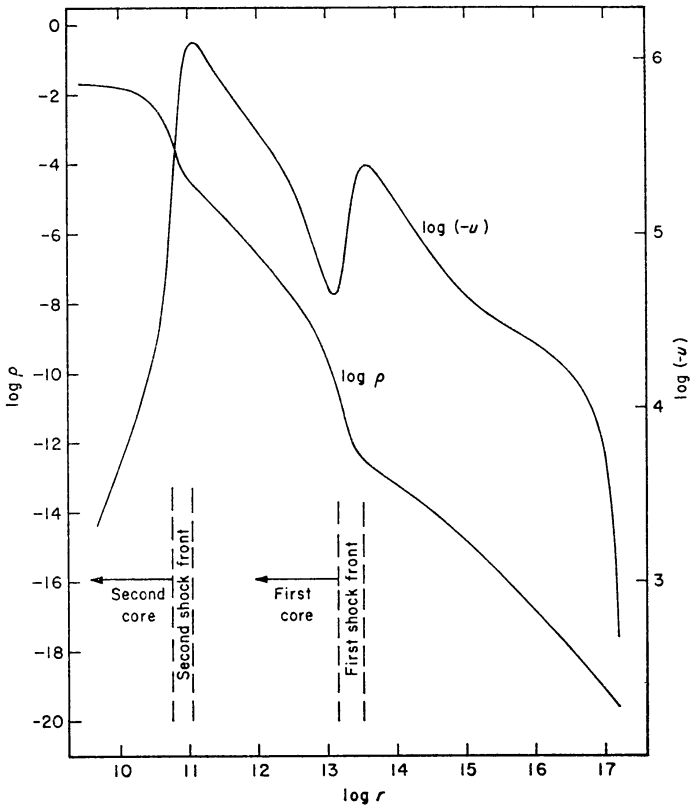

FIG. 2. *The density and velocity distributions at a time shortly after the formation of the second (stellar) core (CGS units). The shock fronts are represented by the regions of steep positive slope in the velocity curve.*

this core, the mass originally constituting the first core becomes rapidly depleted, and the density of the infalling material drops rapidly. Because of the shock jump conditions, the density inside the shock front also drops rapidly, while the temperature decreases only by a relatively small factor; therefore, the specific entropy of the material entering the second core increases, with the result that the core expands in radius. During this initial expansion phase the core radius increases roughly proportionally with its mass, reaching a maximum value of $12\,R_\odot$ when the mass reaches $1{\cdot}0\times10^{-2}\,M_\odot$. At this time, which occurs about 1 yr after the formation of the stellar core, the first shock front is still in existence but is beginning to die out as material falls away from it.

As the core expands, the central temperature and density continually rise, as does the degree of ionization. Because of the high central density, however, the rate of increase of the degree of ionization is insufficient to reduce the ratio of specific heats γ below 4/3, so there is no further dynamical collapse of the core.

The evolution of the stellar core in an HR diagram has been plotted in Fig. 3, where the initial expanding phase of the evolution is represented by the dashed section of the curve. The curve has been drawn dashed because it indicates only the variation in radius and surface temperature of the core; the luminosity indicated by the curve is not an observationally significant quantity, since the radiation emitted from the shock front is completely absorbed in the very opaque material immediately outside the shock front.

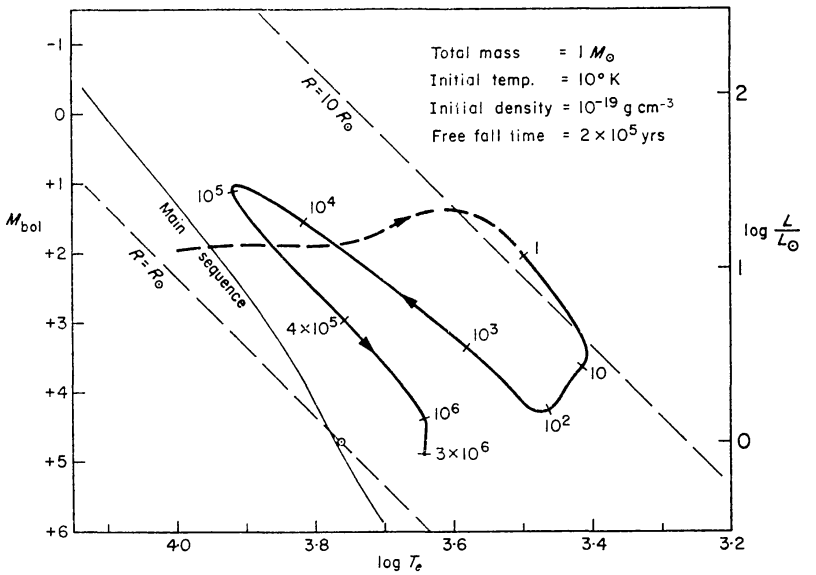

FIG. 3. *The evolution of the stellar core in an HR diagram. The numbers marked along the curve are the times in years since the formation of the stellar core. The dashed section of the curve represents the phase when the luminosity emitted from the core is completely absorbed in the infalling material, and the beginning of the solid curve represents the point where about* 90 *per cent of the luminosity from the core is transmitted outward through the whole proto-stellar cloud. See text for further explanation of the curve.*

(e) *Radiative cooling and contraction of the core*

When the density outside the shock front drops to about 10^{-8} g cm^{-3}, the opacity of the infalling material becomes small enough to allow the energy radiated from the shock front to be transported outward through the infalling material and eventually escape from the cloud altogether. The luminosity of the proto-stellar object then increases rapidly from a very small value to a value of about 10 $L_\odot$, as indicated by the beginning of the solid curve in Fig. 3. Because of the radiative energy loss from the shock front, the specific entropy of the material entering the core begins to decrease, with the result that the core stops expanding and begins to contract. Also, a convection zone appears at the surface of the core and begins to spread inward.

As the temperature and density inside the shock front continue to decrease, the opacity in the surface layers of the core also decreases, eventually becoming small enough for radiative energy transfer to become important. The core then begins to lose a significant amount of energy through the combined effects of convective energy transport from the interior and radiative energy losses from the surface layers; as a result the core contracts by a significant factor in radius. This phase of the evolution, represented in Fig. 3 by the section of the curve

between approximately 10 and 100 years after the formation of the stellar core, is quite analogous to the pre-main sequence contraction of a star along the convective 'Hayashi track'. During this phase of the evolution the core mass increases only slightly to about $1\cdot3\times10^{-2}\,M_\odot$. At the end of this phase all traces of the first core and of the shock front bounding it have disappeared, and there is very little mass left in the innermost part of the collapsing cloud.

It should be noted that, because of the opacity produced by the dust grains in the infalling material, the infalling cloud remains optically thick until practically all of the material has fallen into the core. Thus, although the luminosity emitted from the cloud is the same as the luminosity of the stellar core, the energy leaves the cloud as thermal infra-red emission from the dust grains. The spectrum of the emitted radiation and its variation with time will be considered in a forthcoming paper.

(f) *Main accretion phase*

During the later stages of the collapse, the thermal energy of the material entering the shock front is negligible compared with the kinetic energy. Since the infalling material has been in free fall from an effectively infinite distance, its velocity u_2 just before entering the shock front is given by

$$\frac{1}{2}u_2^2=\frac{GM}{R} \tag{8}$$

where M is the mass and R the radius of the core. Thus as the core contracts, the kinetic energy inflow to the shock front increases, soon becoming greater than the energy outflow from the interior of the core. The dominant terms in the shock front energy equation (A4) then become the kinetic energy inflow and the radiative energy loss terms, so that equation (A4) reduces to

$$\sigma T_e^4=\tfrac{1}{2}\rho_2|u_2|^3 \tag{9}$$

where T_e is the effective temperature of the stellar core and ρ_2 is the density just outside the shock front. Equation (9) simply states that the radiative energy flux leaving the shock front is equal to the kinetic energy flux entering it.

As a result of the increasing surface temperature and the decreasing energy loss from the interior of the core, the specific entropy of the material entering the core eventually stops decreasing and begins to increase. Consequently the core stops contracting and the convection zone in the outer part of the core shrinks and disappears. During the subsequent evolution the core mass increases by a large factor, while the radius changes very little, due to the counteracting effects of increasing specific entropy and increasing mass. Thus the infall velocity u_2 and the core surface temperature and luminosity all increase greatly, in accordance with equations (8) and (9). This is indicated in Fig. 3 by the section of the curve between approximately 10^2 and 10^5 years after the formation of the core.

The radius of the stellar core during the later stages of the collapse is determined primarily by the specific entropy of the material in the outer part of the core, i.e. by the recent history of the accretion process; the early history of the accretion process and the properties of the material in the central part of the core become less and less important as the collapse proceeds. This is fortunate, since it means that the effects of any errors or uncertainties arising in the early

stages of the collapse are damped out as the evolution proceeds and become unimportant for the final results.

(g) *Final stages of the evolution*

When approximately half of the total mass has fallen into the core, the rate of increase of the infall velocity u_2 becomes insufficient to offset the decrease in the infall density ρ_2, and the kinetic energy influx $\frac{1}{2}\rho_2|u_2|^3$ begins to decrease. Consequently the surface temperature and luminosity of the core also begin to decrease, as indicated in Fig. 3 by the section of the curve between approximately 10^5 and 10^6 years. The specific entropy of the material entering the core also begins to decrease, and a convection zone again appears at the surface of the core and begins to spread inward. The maximum surface temperature and luminosity, i.e. about 8300°K and $30\,L_\odot$ respectively, are attained at about 8×10^4 years after the formation of the core, at which time the core mass is $0{\cdot}56\,M_\odot$.

As the surface temperature and luminosity of the core decrease, the opacity in the surface layers of the core also decreases, and the energy outflow from the interior of the core becomes increasingly important. Eventually, after about 10^6 years, when practically all of the proto-stellar mass has fallen into the core, the kinetic energy inflow to the shock front becomes negligible compared with the energy outflow from the interior of the core. The luminosity radiated from the surface of the core then comes primarily from the interior of the core and no longer from the kinetic energy inflow. Thus the stellar core becomes essentially an ordinary star, and its surface layer becomes an ordinary stellar atmosphere. At this time the outer convection zone covers somewhat more than half of the mass and radius of the core, so that in its important features the resulting star is essentially a conventional Hayashi model in the convective phase of pre-main sequence contraction (Hayashi, Hoshi & Sugimoto 1962). The final section of the evolutionary path in Fig. 3, between approximately 10^6 and 3×10^6 years, represents the 'Hayashi track' as far as the present calculations have been carried, and it is in good agreement with previous calculations of the Hayashi track (Ezer & Cameron 1963, 1965; Iben 1965; Bodenheimer 1965, 1966a, 1966b).

When the infall effects become negligible and the star first appears on the Hayashi track, the radius, effective temperature, and luminosity are about $2{\cdot}0\,R_\odot$, 4400°K, and $1{\cdot}3\,L_\odot$, respectively. The time elapsed since the formation of the stellar core is about $1{\cdot}1\times10^6$ years, or about 5 times the initial free-fall time of the cloud. It is noteworthy that, although the resulting star does eventually appear on the Hayashi track, it does so with a radius and luminosity which are much smaller than the very large values of $\sim60\,R_\odot$ and $\sim600\,L_\odot$ which have previously been assumed (Ezer & Cameron 1965). In fact, the star comes onto the Hayashi track with such a small radius and high internal temperature that a central region in radiative equilibrium has already appeared and begun to grow outward. Thus the maximum extent of the outer convection zone, i.e. about 57 per cent of the mass and 56 per cent of the radius, is achieved just as the star comes onto the Hayashi track.

Although the resulting star is outwardly like a conventional Hayashi model, there is actually a small central region of very low specific entropy, i.e. low temperature and high density, as is evident in Fig. 4. The temperature maximum seen in Fig. 4 occurs at about 5 per cent of the mass and 15 per cent of the radius

outward from the centre. The very low central specific entropy has been preserved since the time of formation of the stellar core because radiative energy transport in the central region has remained negligible during the entire evolution of the core. However, the central region of low entropy disappears because of radiative heating before the contracting star reaches the main sequence, and its existence does not appear to have any important consequences for the evolution of the star.

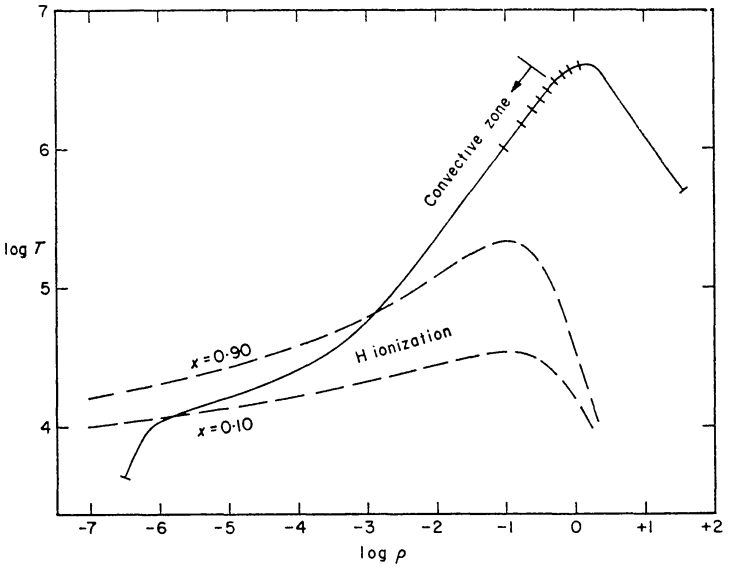

FIG. 4. *The run of log T* vs. *log ρ in the resulting star when it first appears on the Hayashi track. The ticks along the curve divide the star into ten zones of equal mass. The dashed curves are lines of constant degree of ionization x.*

5. RESULTS WITH OTHER ASSUMPTIONS

In view of the many uncertainties in our assumptions and input data, we have repeated the calculations with different choices for some of the important parameters, in order to find their effect on the results. The additional calculations are designated below as Cases 2–7, Case 1 being counted as the one already described in detail in Section 4. In most respects the results in Cases 2–7 are similar to those already described for Case 1, so we shall in the following only indicate the respects in which they differ importantly from Case 1. The initial and final properties of the stellar core are summarized in Tables I and II respectively, for all the cases calculated.

Case 2. In order to find the effect of uncertainty in the assumed initial temperature, a calculation was made with the initial temperature increased by one order of magnitude to 100°K. The corresponding initial density required to ensure collapse is then $1{\cdot}1 \times 10^{-16}$ g cm^{-3}. Up to the time of formation of the stellar core, the collapse proceeds qualitatively much as in Case 1. It is evident in Table I that the initial properties of the stellar core in Case 2 are remarkably similar to Case 1; the main difference is that the collapse time is much shorter, because of the higher initial density. The evolution of the stellar core in an HR diagram is shown in Fig. 5. During most of the evolution, the core surface temperature is higher than in Case 1 because of the higher density of the infalling material and the higher kinetic energy influx. This results in a higher specific

entropy for the material entering the core, and consequently a larger core radius than in Case 1. The properties of the resulting star when it first appears on the Hayashi track are as listed in Table II.

TABLE I

Initial properties of the stellar core

Case No.	t (yrs)	M (g)	R (cm)	ρ_c (g/cm^3)	T_c (°K)
1	3 (+5)	3 (+30)	9 (+10)	2 (−2)	2·2 (+4)
2	9 (+3)	6 (+30)	1·5 (+11)	9 (−3)	2·3 (+4)
3	6 (+3)	4 (+30)	1·0 (+11)	1·7 (−2)	2·2 (+4)
4	3 (+5)	1·5 (+30)	4 (+10)	9 (−2)	2·2 (+4)
5	1·2 (+5)	6 (+31)	5 (+11)	3 (−3)	6 (+4)
6	1·3 (+5)	4 (+30)	1·4 (+11)	2 (−3)	1·9 (+4)
7	5 (+4)	5 (+30)	1·4 (+11)	9 (−3)	2·3 (+4)

TABLE II

Final properties of the stellar core

Case No.	t* (yrs)	$M/M_\odot$	$R/R_\odot$	T_e (°K)	$L/L_\odot$
1	1·1 (+6)	1·0	2·0	4400	1·3
2	3·3 (+4)	1·0	5·1	4300	7·7
3	2·8 (+4)	1·0	5·7	4200	9·2
4	1·1 (+6)	1·0	2·0	4400	1·3
5	4·5 (+5)	1·0	2·5	4400	2·0
6	2·0 (+5)	2·0	5·0	4900	13
7	1·1 (+5)	5·0	7·0	13000	1300

* This is the time after formation of the stellar core.

Case 3. In order to find the effect of increasing the initial density without changing the initial temperature, a calculation was made with an initial temperature of 10°K as in Case 1 but an initial density of $1{\cdot}1 \times 10^{-16}$ g cm^{-3} as in Case 2. The evolution of the stellar core in Case 3 is shown in Fig. 6. It is evident that,

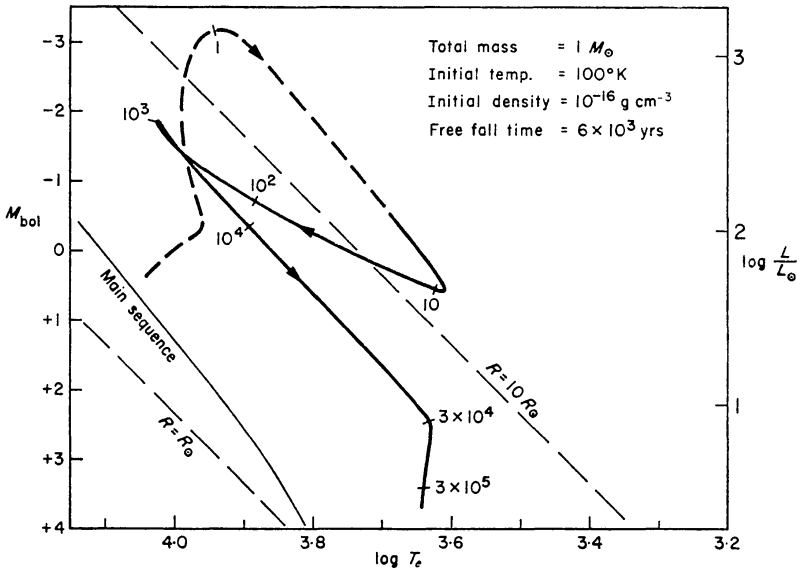

FIG. 5. *The evolution of the stellar core in an HR diagram for Case 2.*

although the evolution starts out much the same as in Case 1, the final stages of the evolution and the properties of the resulting star (Table II) resemble Case 2 more closely than Case 1. This shows that the later stages of the evolution and the properties of the resulting star are determined primarily by the initial density of the proto-stellar cloud; the initial temperature is only of secondary importance, except in so far as it determines the initial density.

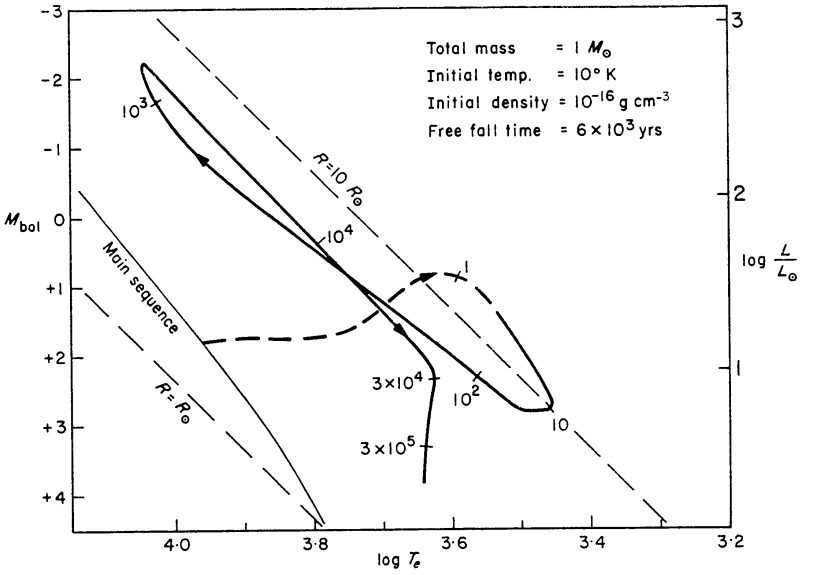

FIG. 6. *The evolution of the stellar core in an HR diagram for Case* 3.

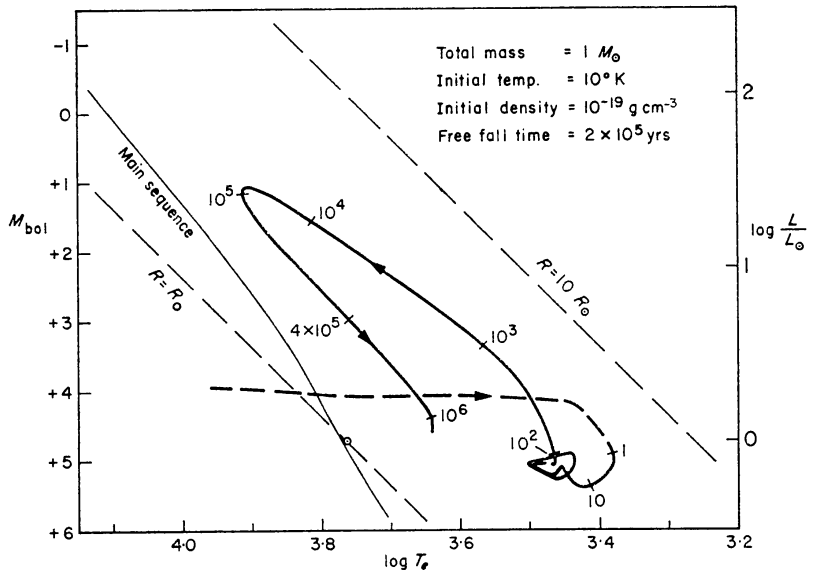

FIG. 7. *The evolution of the stellar core in an HR diagram for Case* 4.

Case 4. In order to find the effect of uncertainty in the assumed dust opacity, and also to obtain an idea of how star formation might proceed in a region of greatly reduced dust content, a calculation was made with the assumed dust opacity reduced by two orders of magnitude to 0·0015 cm^2 g^{-1}; the other parameters were the same as in Case 1. The result is shown in Fig. 7. The core starts out smaller and denser than in Case 1, but during the later stages of the collapse the dust opacity has negligible effect on the dynamics of the collapse, and the

evolution of the core becomes almost indistinguishable from Case 1. This result demonstrates the unimportance of the assumed dust opacity, and it also verifies that the later stages of the evolution of the core are very little dependent on the details of the earlier stages of evolution.

Case 5. To find the importance of the assumption that the hydrogen is initially all molecular, a calculation was made with the extreme assumption that hydrogen molecules never exist at any time. The initial density in this case was $6{\cdot}4\times10^{-19}$ g cm $^{-3}$, which is higher than in Case 1 because of the larger value of the gas constant $\mathscr{R}$. In Case 5 the details of the collapse are somewhat different from the other cases. The central part of the first core does not collapse dynamically

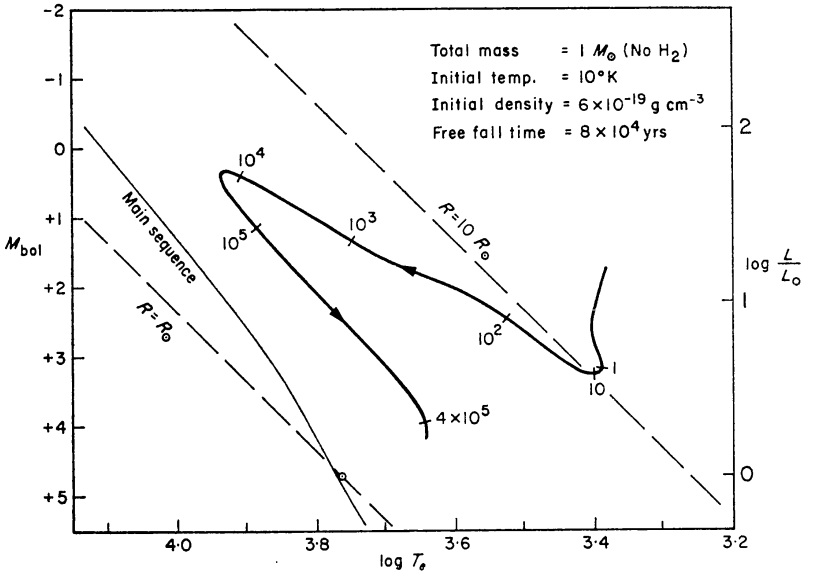

FIG. 8. *The evolution of the stellar core in an HR diagram for Case* 5.

as in the other cases, but instead contracts quasi-statically by a large factor due to radiative energy losses occurring when the dust grains evaporate. Eventually there is a small dynamical collapse at the centre caused by hydrogen ionization; this results finally in the formation of a small stellar core, much as in the other cases. After the disappearance of the outermost shock front the evolution of this stellar core proceeds much as in Case 1 (see Fig. 8). The main differences are a somewhat larger core radius and a shorter time scale; these effects are attributable as in Cases 2 and 3 primarily to the higher initial density of the proto-stellar cloud.

Case 6. This calculation was made with a total mass of 2 $M_\odot$, and with assumptions chosen rather differently from the other cases. The initial temperature and density were 10°K and $2{\cdot}5\times10^{-19}$ g cm^{-3}, respectively, and the boundary condition was taken as $P=$ const. up to the time of formation of the stellar core, and $u=0$ (i.e. a fixed boundary) thereafter. The boundary then contracts by about a factor of 2 in radius during the early stages of the collapse. The evolution of the stellar core is shown in Fig. 9. In Case 6 the resulting star appears almost at the bottom of its Hayashi track, and the outer convection zone at its maximum extent covers only somewhat less than half of the mass and radius of the star. In this case it was possible to follow the evolution of the star almost to the main sequence, as shown by the final section of the curve in Fig. 9. This final section

is not expected to be as accurate as previous pre-main sequence calculations, but it at least verifies that the final stages of the pre-main sequence contraction are essentially the same as previously calculated and are not affected by the details of the dynamical collapse phase.

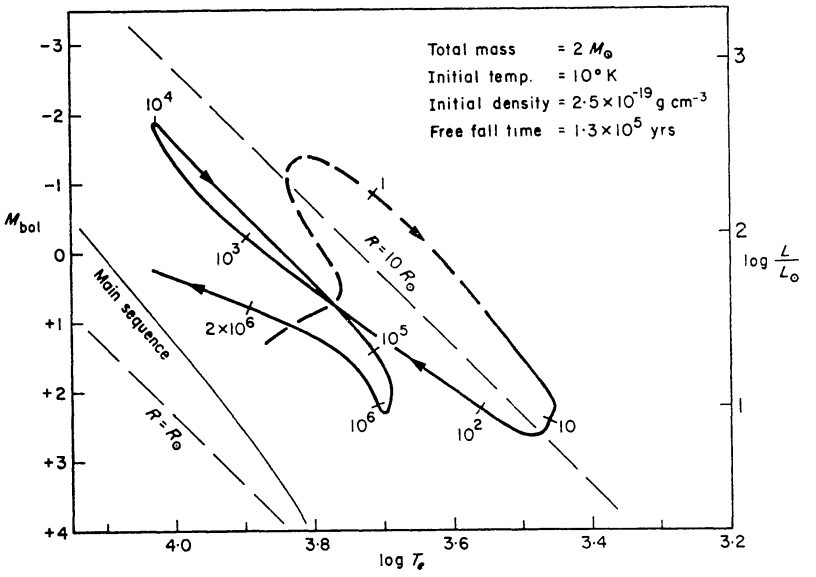

FIG. 9. *The evolution of the stellar core in an HR diagram for Case* 6.

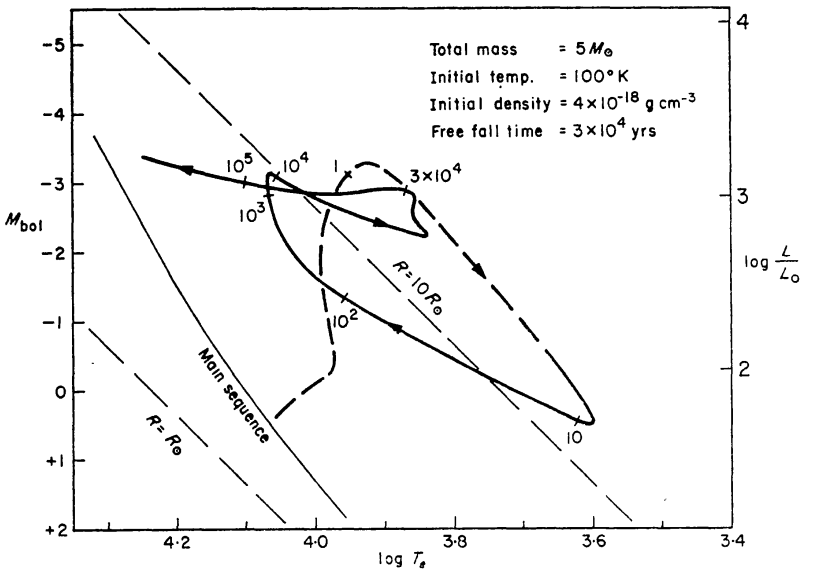

FIG. 10. *The evolution of the stellar core in an HR diagram for Case* 7.

Case 7. This case was calculated with a total mass of 5 $M_\odot$ in order to find the effect of an increase in mass. If an initial temperature of 10 °K had been chosen, the corresponding initial density from equation (2) would have been so low that the temperature would in reality have been much higher than 10 °K. Consequently, since it was desired to have some comparison with one of the previous cases, a temperature of 100 °K was chosen, as in Case 2. The corresponding initial density is then $4\cdot4\times10^{-18}$ g cm^{-3}. It is evident in Fig. 10 that the evolution of the stellar core in Case 7 is initially almost identical to Case 2, but it begins to differ appreciably after about 10^3 years. This occurs because of radiative energy transport in

the interior of the core, which becomes important at this point because of the higher core mass and higher interior temperature. A central region in radiative equilibrium appears, and the core begins to expand as layers farther and farther out from the centre are heated up by radiative energy transport and come into radiative equilibrium. The surface layers of the core come into radiative equilibrium quite rapidly $2{\cdot}3 \times 10^4$ years after the formation of the core, at which time the core mass is $3{\cdot}7\,M_\odot$ and the surface temperature is at a minimum value of 6900°K. Shortly afterward the radiative energy outflow from the interior of the core becomes greater than the kinetic energy inflow to the shock front; thereafter, the core evolves essentially by radiative cooling and contraction toward the main sequence, although it continues to gain mass. The properties of the resulting star when the infall effects have become negligible are as listed in Table II.

It is noteworthy that in Case 7 there is no convective Hayashi phase at all; the core radius never becomes large enough for a convective phase to exist. Since in Case 6 ($M=2M_\odot$) the star came in almost at the bottom of its Hayashi track, it appears that the Hayashi phase does not exist at all for masses much greater than about $2\,M_\odot$; when they first appear such stars will already be closer to the main sequence than the bottom of the Hayashi track.

6. CONCLUSIONS AND COMPARISON WITH OBSERVATIONS

It is evident from the results described in Sections 4 and 5 that, regardless of the assumptions adopted, the collapse of a proto-star is always exceedingly non-homologous, in the sense that a very small fraction of the mass at the centre collapses all the way to stellar densities and reaches hydrostatic equilibrium before most of the cloud has had time to collapse very far from its initial configuration. The subsequent evolution consists not of the overall contraction of a single cloud or stellar object but of the growth in mass of a very small central core or ' embryonic star ' as the surrounding material falls into it. This hitherto unexpected outcome of the calculations differs considerably from the results of previous authors, e.g. Hayashi (1966), who assumed homologous collapse or polytropic density distributions for a collapsing proto-star.

The results of the present calculations show that, apart from unimportant differences, the star resulting at the end of the collapse of a proto-star of one solar mass is essentially a conventional Hayashi pre-main sequence model as discussed by Hayashi *et al.* (1962) and subsequent authors. Prior to the present work, the applicability of these models had never actually been demonstrated on the basis of any calculations of star formation; they had simply been a result of the arbitrary assumption that a star begins its pre-main sequence evolution with a very large radius. The present calculations show, however, that a star of one solar mass first appears on its Hayashi track with a much smaller radius and luminosity than the very large values which have commonly been assumed. This result is not greatly affected even by large changes in the assumed initial conditions. A star of mass greater than $1\,M_\odot$ appears even lower on its Hayashi track, and for masses much greater than $2\,M_\odot$ the radius of the stellar core never becomes large enough for a convective Hayashi phase to exist at all.

It is of interest to compare the predicted properties of newly formed stars with the observed properties of T Tauri stars, which are believed to be very young newly formed stars. The present calculations predict, when the visual opacity of the infalling material is taken into account, that the stellar core remains

completely obscured by dust during most of its evolution and does not begin to become visible as a star until it has almost reached the Hayashi track. Thus the properties of a star when it first becomes visible are approximately those listed in Table II as the final properties of the stellar core.

The properties of T Tauri stars have recently been reviewed by Kuhi (1966) and Herbig (1967). The distribution of T Tauri stars in the HR diagram, as shown for example by Herbig (1967), is in good general agreement with the prediction that newly formed stars of moderate mass should first appear near the lower end of their Hayashi tracks. It is interesting to note in Herbig's diagram a considerable number of T Tauri stars with radii near $2\,R_\odot$, the predicted radius for a new star of $1\,M_\odot$. Because of the many uncertainties, both theoretical and observational, this agreement is probably fortuitous, but it may at least be an indication that our results are not too seriously in error.

The photometric observations of Mendoza (1966, 1968) show that most T Tauri stars have considerable excess infra-red emission, sometimes to the extent that a large fraction of the total luminosity is emitted in the infra-red. This is in fact just what would be expected for a newly formed star which is still partially obscured by the dust in the infalling material; this dust absorbs some of the stellar radiation and re-emits it thermally at infra-red wavelengths. The problem of the expected spectral energy distribution of such an object, along with the problem of the spectral appearance of a proto-star during the earlier stages when the infalling material is still completely opaque, will be considered in a forthcoming paper.

With regard to the spectroscopic properties of T Tauri stars, it is particularly interesting that in some of the fainter T Tauri-like stars Walker (1961, 1963, 1964) has observed absorption lines redshifted by 150 to 300 km s^{-1}, indicating infall of material into the star. The observed velocities are of the same order as the infall velocities found in the calculations, so it may be that the predicted infall of material is actually observed in some stars. The fact that only relatively few faint T Tauri stars seem to show the effect may mean that the infall effects are observable for only a relatively short time while the star is still heavily obscured by the surrounding material; most of the T Tauri characteristics, on the other hand, may persist for some time after the infall effects have become negligible.

Another effect which according to Walker appears to be related to the infall of material is strong continuous emission in the ultra-violet part of the spectrum. Possibly this effect could, at least partially, be caused by the continuous free–free emission expected from the very hot (up to 10^7 °K) material just inside the shock front bounding the stellar core in our model.

The other properties of T Tauri stars, such as the chromospheric-type emission lines, continuous emission across the spectrum, ejection of material, and irregular variability may also be related to the infall of material, as was originally thought; however, it now seems more likely that in most cases they have their origin in the very violent convective and chromospheric activity which appears to be indicated for T Tauri stars.

ACKNOWLEDGMENT

I am indebted to Dr G. Münch for originally suggesting this project and for many helpful discussions throughout the course of this work. I would like also to acknowledge helpful discussions with Drs R. F. Christy and J. I. Castor

on theoretical and computational aspects of the problem. This work has been supported in part through NSF grant GP–7030.

Mount Wilson and Palomar Observatories, Carnegie Institution of Washington, California Institute of Technology.

Present address:
Yale University Observatory, New Haven, Connecticut 06520.

REFERENCES

Aller, L. H., 1963. *The Atmospheres of the Sun and Stars*, Ronald Press, New York.
Bodenheimer, P., 1965, *Astrophys. J.*, **142**, 451.
Bodenheimer, P., 1966a. *Astrophys. J.*, **144**, 103.
Bodenheimer, P., 1966b. *Astrophys. J.*, **144**, 709.
Bodenheimer, P. & Sweigart, A., 1968. *Astrophys. J.*, **152**, 515.
Cox, A. N., 1966. Unpublished opacity table supplied privately to P. R. Demarque for the composition ' Demarque I '.
Ezer, D. & Cameron, A. G. W., 1963. *Icarus*, **1**, 422.
Ezer, D. & Cameron, A. G. W., 1965. *Can. J. Phys.*, **43**, 1487.
Gaustad, J. E., 1963. *Astrophys. J.*, **138**, 1050; see also unpublished Ph.D. thesis, Princeton University, 1962.
Hayashi, C., 1966. *A. Rev. Astr. Astrophys.*, **4**, 171.
Hayashi, C., Hoshi, R. & Sugimoto, D., 1962. *Progress Theor. Phys. Suppl.*, **No. 22**.
Hayashi, C. & Nakano, T., 1965. *Progress theor. Phys.*, **34**, 754.
Herbig, G. H., 1967. *Scient. Am.*, **217**, No. 2, 30.
Iben, I., 1965. *Astrophys. J.*, **141**, 993.
Kuhi, L. V., 1966. *J. R. astr. Soc. Can.*, **60**, 1.
Liepmann, H. W. & Roshko, A., 1957. *Elements of Gasdynamics*. Wiley and Sons, New York, Ch. 2.
McCrea, W. H., 1957. *Mon. Not. R. astr. Soc.*, **117**, 562.
Mendoza, E. E., 1966. *Astrophys. J.*, **143**, 1010.
Mendoza, E. E., 1968. *Astrophys. J.*, **151**, 977.
Penston, M. V., 1966. *R. Obs. Bull.*, **No. 117**, 299.
Tsuji, T., 1966. *Publ. astr. Soc. Japan*, **18**, 127.
Walker, M. F., 1961. *Comptes Rendus*, **253**, 383.
Walker, M. F., 1963. *Astrophys. J.*, **68**, 298.
Walker, M. F., 1964. *R. Obs. Bull.*, **No. 82**, p. 69.

APPENDIX A

TREATMENT OF THE SHOCK FRONT

In this appendix we outline the approximations which we have adopted in the shock fitting method used during the later stages of the collapse to treat the shock front bounding the stellar core. We require a set of equations analogous to the ordinary adiabatic shock jump equations, which relate the values of the flow variables at two points just inside and outside the shock front. We shall denote quantities evaluated at a suitably chosen point inside the shock front by a subscript 1, and quantities at a point outside the shock front by a subscript 2. We assume that the flow through the shock front may be treated as a steady flow, and that the velocity of the shock front may be neglected in comparison with the velocity of the infalling material. The mass conservation relation for the shock region can then be written down immediately:

$$\rho_1 u_1 = \rho_2 u_2. \tag{A1}$$

We now derive an energy conservation relation for the shock region by considering the various energy inflow and outflow rates across the two surfaces

bounding the shock region. First of all, we have the ordinary mechanical energy transport rates, consisting of an energy inflow to the shock front of $\rho_2|u_2|(H_2+\frac{1}{2}u_2^2)$ and an energy outflow of $\rho_1|u_1|(H_1+\frac{1}{2}u_1^2)$, where H denotes the specific enthalpy (see for example Liepmann & Roshko, 1957). In the present problem it is necessary also to take into account radiative energy transport into and out of the shock region. The outward energy flux F_1 from the interior of the core counts as an energy input to the shock region, and it is related in a known way to the temperature gradient in the surface layers of the core. The radiative flux F_2 emitted outward from the shock front depends on the temperature distribution inside the shock front, but for the present purposes we would like to relate F_2 to the single parameter T_1, which we take to be the limiting temperature reached inside the shock front after radiative cooling has become negligible.

During the important later stages of the collapse the temperature immediately inside the shock jump becomes extremely high due to the high kinetic energy of the infalling material; radiative cooling then reduces the temperature by a large factor as the material moves inward from the shock jump. Under these circumstances it becomes a difficult problem to relate the emitted flux F_2 to the limiting temperature T_1 inside the shock front. We know however that the effective temperature T_e defined by $F_2=\sigma T_e^4$ must be intermediate between the peak temperature and T_1, and closer to the latter. In fact it can be shown (see Appendix B) that no matter how high the peak temperature is we must always have

$$T_1 < T_e < 1\cdot 28\, T_1. \tag{A2}$$

Since high accuracy is not a consideration in the present project, we have considered it an adequate approximation to simply set

$$T_e = T_1. \tag{A3}$$

The desired energy conservation relation for the shock region can then be written as follows, collecting the various energy gain and loss terms:

$$\rho_1|u_1|(H_1+\tfrac{1}{2}u_1^2)+\sigma T_1^4=\rho_2|u_2|(H_2+\tfrac{1}{2}u_2^2)+F_1. \tag{A4}$$

We now consider the shock momentum equation, which is important for determining the pressure P_1 inside the shock front. During the later stages of the evolution when the region inside the shock front becomes essentially a stellar atmosphere, it becomes important that P_1 refer not to a point immediately inside the shock jump, but to a point at an optical depth of order unity inside the shock jump, which can serve as a suitable photospheric boundary point for the core model. A common procedure in stellar interiors calculations is to choose the photospheric boundary point to be that point where the actual temperature is equal to the effective temperature; according to the Eddington approximation, this occurs at an optical depth of $2/3$. If we integrate the hydrostatic equilibrium equation $dP/d\tau=g/\kappa$ between $\tau=0$ and $\tau=2/3$, assuming $\kappa\propto P^{1/2}$, we find that the photospheric pressure P_1 is greater than the pressure immediately inside the shock jump by approximately an amount g/κ_1. We have added this term to the usual adiabatic shock momentum equation to obtain the following approximate relation applicable to the present problem:

$$P_1+\rho_1 u_1^2 = P_2+\rho_2 u_2^2+\frac{g}{\kappa_1}. \tag{A5}$$

With equations (A1), (A4), and (A5) we now have the three equations required to relate the values of all of the variables on the two sides of the shock front.

APPENDIX B

PROOF OF EQUATION (A2)

This proof will be based on the following equation relating the two radiation integrals K and H for the grey case (see Aller 1963, p. 223):

$$\frac{dK}{d\tau} = H. \tag{B1}$$

We shall denote by a subscript s the values of the variables right at the shock jump and by a subscript 1 the values at a suitable point inside the shock front, as in Appendix A. Applying equation (B1) in the region inside the shock jump, we have, since the net radiative flux is always outward, $H>0$ and $dK/d\tau>0$; therefore, we must have

$$K_1 > K_s. \tag{B2}$$

We assume that the point 1 is at a sufficiently large optical depth that the radiation intensity is isotropic and equal to the blackbody intensity $B(T_1)$. We then have $K_1 = \frac{1}{3}B(T_1)$, and consequently from equation (B2)

$$\tfrac{1}{3}B(T_1) > K_s. \tag{B3}$$

From the definitions of K and H and a consideration of the possible forms for the angular dependence of the radiation intensity $I(\theta)$, it can be shown that the smallest possible ratio of K_s to H_s is obtained when $I_s(\theta)\propto(\cos\theta)^{-1}$, in which case $K_s = \frac{1}{2}H_s$. Substituting this lower limit for K_s into equation (B3), we obtain

$$\tfrac{1}{3}B(T_1) > \tfrac{1}{2}H_s. \tag{B4}$$

Finally, making use of the definition of T_e we have

$$H_s = \frac{F_s}{4\pi} = \frac{\sigma T_e^4}{4\pi} = \tfrac{1}{4}B(T_e). \tag{B5}$$

Substituting this into equation (B4), we have

$$\tfrac{1}{3}B(T_1) > \tfrac{1}{8}B(T_e)$$

or

$$T_1^4 > \tfrac{3}{8}T_e^4. \tag{B6}$$

Since T_e must be greater than T_1, we can now write

$$T_1^4 < T_e^4 < \tfrac{8}{3}T_1^4$$

or

$$T_1 < T_e < 1\cdot 28 T_1. \qquad \text{Q.E.D.} \tag{B7}$$

The physical reason why T_e can never differ much from T_1 is readily understood. We know that the hot material just inside the shock jump emits a radiative flux of σT_e^4 in the outward direction; a similar amount of energy must also be radiated *inward*, and, therefore, the mean radiation intensity inside the shock front must be of the same order as that for a blackbody of temperature T_e. Consequently the limiting temperature T_1 inside the shock front cannot be very much smaller than T_e.

The above derivation is valid for the grey case, in which the absorption coefficient is assumed to be independent of wavelength. It appears unlikely, however, that the result would be altered by the wavelength dependence of the absorption coefficient expected in the real case.

APPENDIX C

ASYMPTOTIC SIMILARITY SOLUTION FOR THE ISOTHERMAL COLLAPSE OF A SPHERE

In this investigation of the collapse of a proto-star, it has been noted that during the initial isothermal phase of the collapse the density and velocity distributions in the inner part of the collapsing cloud appear to approach constant limiting forms, with the time dependence given only by scale factors which vary as a function of time. This suggests that there may exist an asymptotic 'similarity' solution for the isothermal collapse of a sphere. In this appendix we show that this is indeed the case, and we present some numerical results for this asymptotic solution. We also show that the similarity solution may be generalized to the case of a polytropic equation of state $P = K\rho^{\gamma}$ and we use this to indicate the effects of deviations from isothermality in the collapse.

In Eulerian form, the equations governing the isothermal collapse may be written

$$\frac{\partial u}{\partial t}+u\frac{\partial u}{\partial r}+\frac{Gm}{r^2}+\mathscr{R}T\frac{d\ln\rho}{dr}=0,$$

$$\frac{\partial m}{\partial t}+4\pi r^2\rho u=0, \tag{C1}$$

$$\frac{\partial m}{\partial r}-4\pi r^2\rho=0,$$

where T is fixed and m is the mass within a sphere of radius r. Suppose that at any given time t_1 the velocity, density and mass distributions are given by $u_1(r)$, $\rho_1(r)$ and $m_1(r)$. We then seek a solution of equations (C1) in which at a general time t the velocity, density and mass distributions have the forms

$$\begin{aligned} u(r,t) &= b(t)u_1(s),\\ \rho(r,t) &= c(t)\rho_1(s),\\ m(r,t) &= d(t)m_1(s), \end{aligned} \tag{C2}$$

where

$$s = r/a(t).$$

Here $a(t)$, $b(t)$, $c(t)$, and $d(t)$ are dimensionless scale factors which depend only on time, and are equal to unity at time t_1. Substitution of equations (C2) into equations (C1) shows that such a solution is possible if the following relations hold:

$$b(t)=1, \qquad c(t)=a(t)^{-2}, \qquad d(t)=a(t). \tag{C3}$$

Since the initial and boundary conditions for the collapsing cloud of course do *not* vary in accordance with equations (C2), and (C3), it is clear that a solution of the above form can be valid only as a limiting approximation in the case where the initial and boundary conditions can be considered as infinitely far removed and no longer influencing the solution in the region of interest.

Substituting equations (C2), and (C3), into equations (C1), we obtain 3 simultaneous ordinary differential equations for the functions $u_1(s)$, $\rho_1(a)$ qnd $m_1(s)$ After some straightforward substitutions to eliminate m_1 in favour of u_1 and ρ_1, thus

reducing the number of equations from 3 to 2, we obtain

$$\left(\frac{s}{\tau}+u_1\right)\frac{du_1}{ds}+4\pi G\rho_1(s+u_1\tau)+\mathscr{R}T\frac{d\ln\rho_1}{ds}=0,$$
$$\frac{du_1}{ds}+\left(\frac{s}{\tau}+u_1\right)\left(\frac{d\ln\rho_1}{ds}+\frac{2}{s}\right)=0, \tag{C4}$$

where $\tau=-(da/dt)^{-1}$ is a fixed (positive) constant independent of both r and t.

For further analysis it is convenient to reduce these equations to non-dimensional form by means of the following transformations:

$$x=\frac{s}{\tau\sqrt{(\mathscr{R}T)}},\qquad \xi=\frac{-u_1}{\sqrt{(\mathscr{R}T)}},\qquad \eta=4\pi G\rho_1\tau^2. \tag{C5}$$

If we substitute these relations into equations (C4) and solve for $d\xi/dx$ and $d\ln\eta/dx$, we obtain

$$\frac{d\xi}{dx}=\frac{x-\xi}{x}\frac{\eta x(x-\xi)-2}{(x-\xi)^2-1},$$
$$\frac{d\ln\eta}{dx}=\frac{x-\xi}{x}\frac{\eta x-2(x-\xi)}{(x-\xi)^2-1}. \tag{C6}$$

A unique solution for this set of equations is determined by the following two conditions: (1) $\xi=0$ at $x=0$, and (2) $\eta x=2$ at $x-\xi=1$, the latter condition being required to avoid a physically inadmissible singularity at $x-\xi=1$.

Before presenting the numerical solution of equations (C6), we note that the limiting behaviour of the solution for large and small x is readily found directly from the equations. The case of most interest is $x\gg 1$, since this is the limit approached at any fixed value of r as the collapse progresses and $a(t)$ decreases. Putting $x\gg 1$ in equations (C6) and making use of the facts that $x-\xi\to\infty$ and $\eta\to 0$ as $x\to\infty$, we find

$$\left.\begin{aligned}\frac{d\ln\xi}{d\ln x}&\to 0\\ \frac{d\ln\eta}{d\ln x}&\to -2\end{aligned}\right\}\ \text{as } x\to\infty. \tag{C7}$$

Consequently $u(r)$ approaches a constant and $\rho(r)$ approaches the form $\rho\propto r^{-2}$ as the collapse proceeds. These properties of the isothermal collapse solutions were noted by Bodenheimer & Sweigart (1968) and also in the present paper (see Fig. 1).

We have solved equations (C6) numerically by using a Runge–Kutta scheme and proceeding outward from the centre ($x=0$), trying various values of $\eta(0)$ until a solution was found satisfying the condition $\eta x=2$ at $x-\xi=1$. The resulting solution is illustrated in Fig. C1. The limiting forms of this numerical solution are as follows:

$$\text{for } x\ll 1,\quad \xi=\tfrac{2}{3}x,\quad \eta=1\cdot 667;$$
$$\text{for } x\gg 1,\quad \xi=3\cdot 28,\quad \eta=8\cdot 86x^{-2}. \tag{C8}$$

Numerical calculations of the isothermal collapse of a sphere carried out using the methods of this paper have verified that the density and velocity distributions in the collapsing cloud do indeed approach the asymptotic forms

derived above, at least within the accuracy of the calculations (≈ 10 per cent). As was noted by Bodenheimer & Sweigart (1968), the solution has this character only if the collapse time exceeds the time required for sound to travel inward from the surface to the centre of the cloud, but this is in fact usually the case if the initial conditions are approximately in accordance with the virial theorem. After the central density has risen by 4 or 5 orders of magnitude, the approximate

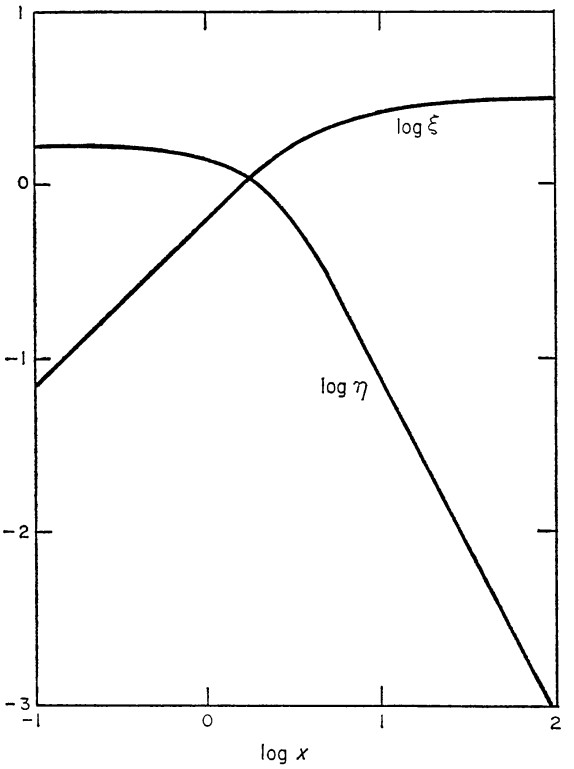

FIG. C1. *The numerically computed similarity solution for isothermal collapse (see equation (C5) for the definitions of the variables).*

density law $\rho \propto r^{-2}$ is already well established over a significant part of the collapsing cloud (see for example Fig. 1). The infall velocity also becomes roughly constant over a significant part of the cloud, as predicted by the similarity solution, but the velocity distribution approaches the similarity solution only slowly and the collapse must be followed through at least 12 orders of magnitude in density before the maximum velocity comes within 10 per cent of the value $3{\cdot}28\sqrt{(\mathscr{R}T)}$ predicted by the similarity solution.

It is noteworthy that, although the collapse proceeds qualitatively like a free fall, pressure gradient forces are *not* negligible and in fact are of essential importance in determining the form of the solution. The ratio of pressure gradient to gravitational forces in the similarity solution may be straightforwardly obtained from equations (C4), (C5), and (C6); the result may be written

$$\left|\frac{\text{pressure}}{\text{gravity}}\right| = \frac{|d \ln \eta/dx|}{\eta(x-\xi)} = \frac{2(x-\xi)/\eta x - 1}{(x-\xi)^2 - 1}. \qquad \text{(C9)}$$

The limiting values of this ratio may be found by substituting the limiting forms

of ξ and η from equations (C8); this gives

$$\begin{aligned} &\text{for } x \ll 1, \quad \left|\frac{\text{pressure}}{\text{gravity}}\right| = 0{\cdot}600; \\ &\text{for } x \gg 1, \quad \left|\frac{\text{pressure}}{\text{gravity}}\right| = 0{\cdot}226. \end{aligned} \tag{C10}$$

Thus for example at the centre of the collapsing cloud the actual acceleration is only 0·400 times the gravitational acceleration, and the collapse time scale is longer than the free-fall time by a factor of $(0{\cdot}400)^{-1/2} = 1{\cdot}58$.

We note in passing that the extremely non-homologous character of the collapse and the importance of pressure gradients in the collapse calculations casts doubt on the validity of analyses of collapse and/or fragmentation which have neglected pressure effects.

It may be noted that the asymptotic similarity solution which we have derived depends only on the gas constant $\mathscr{R}$ and the temperature T of the collapsing cloud, and not on any other properties of the cloud. Thus for clouds with the same $\mathscr{R}$ and T, the collapse solution in the inner part of the cloud should eventually approach the same behaviour in all cases, regardless of such factors as the initial density or the mass of the cloud. This explains the close similarity found between Cases 1 and 3 and also between Cases 2 and 7 in the formation and early evolution of the stellar core in a collapsing proto-star.

It can be shown, by a derivation similar to but somewhat more involved than that presented here, that the similarity solution can be generalized to the case of a polytropic equation of state, i.e. $P = K\rho^{\gamma}$. Again the limiting behaviour of the solution at large x may be obtained directly from the equations. The result is

$$\left.\begin{aligned} &\frac{d\ln\xi}{d\ln x} \to \frac{1-\gamma}{2-\gamma} \\ &\frac{d\ln\eta}{d\ln x} \to \frac{-2}{2-\gamma} \end{aligned}\right\} \quad \text{as } x \to \infty, \tag{C11}$$

where x, ξ and η are defined by equations (C5) with $\mathscr{R}T$ replaced by $K(4\pi G\tau^2)^{1-\gamma}$. Equations (C7) are then seen to be a special case of equations (C11) for $\gamma = 1$. Equations (C11) with $\gamma \neq 1$ allow us to see the effects of deviations from isothermality in the collapse. If, for example, the temperature increases with increasing density, corresponding to $\gamma > 1$, we have $d\ln\eta/d\ln x < -2$, i.e. the density gradient becomes *steeper* than in the isothermal case. Conversely the effect of a decreasing temperature is to make the density gradient less steep than in the isothermal case. These properties of the solution and the limiting slopes predicted by equations (C11) have again been verified by numerical collapse calculations made assuming several different values of γ.